Appl. Math. Mech. -Engl. Ed., **42**(6), 855–870 (2021)

APPLIED MATHEMATICS AND MECHANICS (ENGLISH EDITION)

https://doi.org/10.1007/s10483-021-2742-9

Nonlocal thermoelastic analysis of a functionally graded material microbeam*

Wei PENG[1], Like CHEN[2], Tianhu HE[1,3,†]

1. Key Laboratory of Disaster Prevention and Mitigation in Civil Engineering of Gansu Province, Lanzhou University of Technology, Lanzhou 730050, China;
2. School of Civil Engineering and Mechanics, Lanzhou University, Lanzhou 730000, China;
3. School of Science, Lanzhou University of Technology, Lanzhou 730050, China

(Received Jan. 17, 2021 / Revised Mar. 17, 2021)

Abstract In extreme heat transfer environments, functionally graded materials (FGMs) have aroused great concern due to the excellent thermal shock resistance. With the development of micro-scale devices, the size-dependent effect has become an important issue. However, the classical continuum mechanical model fails on the micro-scale due to the influence of the size-dependent effect. Meanwhile, for thermoelastic behaviors limited to small-scale problems, Fourier's heat conduction law cannot explain the thermal wave effect. In order to capture the size-dependent effect and the thermal wave effect, the nonlocal generalized thermoelastic theory for the formulation of an FGM microbeam is adopted in the present work. For numerical validation, the transient responses for a simply supported FGM microbeam heated by the ramp-type heating are considered. The governing equations are formulated and solved by employing the Laplace transform techniques. In the numerical results, the effects of the ramp-heating time parameter, the nonlocal parameter, and the power-law index on the considered physical quantities are presented and discussed in detail.

Key words nonlocal thermoelastic theory, functionally graded material (FGM), size-dependent microbeam, ramp-type heating, dynamic response

Chinese Library Classification O343.6
2010 Mathematics Subject Classification 74F05

1 Introduction

Functionally graded materials (FGMs)[1–3] are advanced composite materials whose constituents vary smoothly and continuously along certain directions. The FGM structures are

* Citation: PENG, W., CHEN, L. K., and HE, T. H. Nonlocal thermoelastic analysis of a functionally graded material microbeam. *Applied Mathematics and Mechanics* (*English Edition*), **42**(6), 855–870 (2021) https://doi.org/10.1007/s10483-021-2742-9

† Corresponding author, E-mail: heth@lut.edu.cn

Project supported by the National Natural Science Foundation of China (Nos. 11972176 and 12062011) and the Incubation Programme of Excellent Doctoral Dissertation-Lanzhou University of Technology

designed to meet the expected functional requirements, based on the flexible design principles of component parameters and mechanical properties to satisfy the application requirements for many engineering problems. Meanwhile, the booming development of micro/nano science motivates widespread applications of micro/nano electromechanical systems, in which micro- and nano-scale structures such as microbeam, nanotube, and graphene sheet have been widely used as resonators[4], switches[5], sensors[6], actuators[7], and probes[8] due to low weight, small size, and high durability. In the micro/nano engineering communities, FGM micro/nano-structures have also been utilized in micro/nano electromechanical systems to improve thermal resistance and crack resistance. So far, many studies on the mechanical responses of FGMs such as buckling[9–10], bending[11–12], and vibration[13–14] have been conducted.

As proved by the experimental tests[15–22], for micro/nano structures, the size-dependent effect plays an important role in their mechanical performances. The classical continuum mechanics is the most common theory to study the response of structural mechanics. Nevertheless, because the constitutive equation lacks the scale parameter of materials, the classical continuum mechanics cannot capture the size-dependent effect in the micro/nano-structures[23]. In order to describe such a size-dependent effect simply and accurately, the classic continuum mechanics theory has been extended to new theories, for instance, Eringen's nonlocal theory[24], Aifantis's strain gradient theory[25], and Yang's modified couple stress theory[26]. Among them, Eringen's nonlocal theory is the most mature and widely used one, which holds that the stress at one point relies on the strains at all points in the body, and such correlation decreases with the distance. In this theory, the nonlocal parameter was introduced to quantify the contribution of the strain at each point in the deformed body to the stress at a certain point. Peddieson et al.[27] showed that Eringen's nonlocal theory could be potentially employed in nanotechnology. So far, scholars have done many studies on the vibration, bending, and wave propagation of micro- and nano-scale structures in the deformation field[28–33]. They concluded that Eringen's nonlocal theory plays an important role in the design of micro/nano structures. From the aforementioned literature review, it can be realized that the size-dependent related investigations were mainly conducted under the case of single elastic deformation field, lacking the thermoelastic coupling investigations under the case of interactions between the displacement field and the variable temperature field. Nevertheless, it is more important for micro/nano devices to consider the thermal induced stress and deformation in the heat transfer environments.

For elastic structures subject to transient heating loads, the thermal-induced deformation and stress may cause them to be unstable and even damaged. To describe the thermoelastic interactions, the classical coupled thermoelastic theory proposed by Biot[34] predicts that heat transports at an infinite speed due to the nature of Fourier's law. However, it is not consistent with the experimental results[35]. To eliminate such a paradox, based on the Cattaneo-Vernotte (C-V) thermal wave model[36] and the classic elastic relationship, the generalized thermoelastic theories have been subsequently developed by Lord and Shulman[37], Green and Lindsay[38], and Green and Naghdi[39–40]. Based on these theories, a number of works on the thermoelastic dynamic responses[41–43], the mass diffusion[44–46], the wave propagation[47–48], and the magnetic field effect[49–50] have been contributed. Specifically, Ma and He[51] analyzed the dynamic characteristic of an FGM piezoelectric rod heated by a moving heat source. Meanwhile, Li and He[52] studied the dynamic response for an FGM semi-infinite rod subject to an ultrashort laser heat source.

Although many studies are available on the static mechanical behaviors for size-dependent FGM micro/nano-structures in the single deformation field[9–14], no work has completely studied the dynamic response of thermoelastic coupling problems. Nevertheless, it is inevitable for micro/nano-structures suffering a changeable temperature. As a consequence, the thermal-induced stress or deformation occurs, which are worth being fully concerned. This work aims at studying a transient thermoelastic behavior of an FGM microbeam under the nonlocal generalized thermoelasticity. At the left end of the microbeam, the medium is heated by a ramp-type heating load. The corresponding governing equations are formulated and then solved by the Laplace transformation method. In calculation, the distribution of the dimensionless temperature, stress, deflection, and displacement with the change of the ramp-heating time parameter, the nonlocal parameter, and the power-law index are examined and discussed in detail.

2 Theoretical formulations

2.1 Nonlocal continuum mechanics model

In the nonlocal elasticity theory[24], the stress-strain relation can be written as

$$\sigma_{ij}(x) = \int_V K(x, x', \chi)\sigma'_{ij}(x')\mathrm{d}V(x'), \tag{1}$$

$$\sigma'_{ij}(x') = \lambda\varepsilon'_{kk}(x')\delta_{ij} + 2\mu\varepsilon'_{ij}(x'), \tag{2}$$

$$\varepsilon'_{ij}(x') = \frac{1}{2}\Big(\frac{\partial u'_j(x')}{\partial x'_i} + \frac{\partial u'_i(x')}{\partial x'_j}\Big), \tag{3}$$

where $\sigma_{ij}(x)$ and $\sigma'_{ij}(x')$ are the nonlocal and classical stress components, respectively. $\varepsilon'_{ij}(x')$ is the classical strain component, ε'_{kk} is the local cubic dilation, $u'_j(x')$ is the local displacement component, and λ and μ are Lamé's constants. The kernel function $K(x, x', \chi)$ depends on the distance $\Delta = \|x-x'\|$ and the material constant $\chi = e_0a/l$, where a is the internal characteristic length scale, l is the external feature length scale, e_0 is a material-dependent constant, and e_0a is the nonlocal parameter.

The integral constitutive equation (1) may be simplified as follows[24]:

$$(1 - (e_0a)^2\nabla^2)\sigma_{ij}(x) = \sigma'_{ij}(x'), \tag{4}$$

where ∇^2 is the Laplacian operator. If a is neglected, Eq. (4) reduces to the constitutive equation in the classical thermoelastic theory.

2.2 Nonlocal generalized thermoelastic model

The basic equations based on nonlocal generalized thermoelasticity[53] are as follows.

The motion equation is

$$\sigma_{ij,j} = \rho\ddot{u}_i, \tag{5}$$

where ρ is the density.

The nonlocal constitutive equation of stress is

$$(1 - (e_0a)^2\nabla^2)\sigma_{ij} = 2\mu\varepsilon_{ij} + \lambda\varepsilon_{kk}\delta_{ij} - (3\lambda + 2\mu)\alpha_{\mathrm{T}}\theta\delta_{ij}, \tag{6}$$

where θ is the temperature above the uniform reference temperature T_0, α_{T} is the coefficient of linear thermal expansion, and δ_{ij} is the Kronecker delta.

The displacement-strain relation is

$$\varepsilon_{ij} = \frac{1}{2}(u_{i,j} + u_{j,i}), \tag{7}$$

where u_i is the displacement component. Lamé's constants can be expressed as

$$\lambda = \frac{E\nu}{(1+\nu)(1-2\nu)}, \quad \mu = \frac{E}{2(1+\nu)}, \tag{8}$$

in which E is the elastic modulus, and ν is Poisson's ratio.

Combining Eqs. (8) and (6) leads to

$$(1 - (e_0a)^2\nabla^2)\sigma_{ij} = \frac{E}{1+\nu}\varepsilon_{ij} + \frac{E\nu}{(1+\nu)(1-2\nu)}\varepsilon_{kk}\delta_{ij} - \frac{E\alpha_{\mathrm{T}}}{1-2\nu}\theta\delta_{ij}. \tag{9}$$

The non-Fourier thermal conduction equation is[37]

$$\kappa \nabla^2 \theta = \Big(1 + \tau_0 \frac{\partial}{\partial t}\Big)(\rho c_{\mathrm{E}} \dot{\theta} + \beta T_0 \dot{\varepsilon}_{kk}), \tag{10}$$

where κ is the thermal conductivity, τ_0 is the thermal relaxation time, c_{E} is the specific heat, and $\beta = E\alpha_{\mathrm{T}}/(1-2\nu)$.

3 Structure modeling

3.1 Problem formulation

As displayed in Fig. 1, an FGM microbeam with a rectangular cross section with length l, width b, and height h is considered, whose cross-sectional area is $A = b \times h$. The (x, y, z) coordinate system is set, where the xy-plane is placed on the neutral surface of the microbeam, and the origin of the coordinate system is located at the centroid of the left end. The x-axis is along the axial direction, the y-axis is along the width direction, and the z-axis is along the thickness direction. Assume that the displacements along the x- and y-directions and the deflection along the z-direction are u, v, and w, respectively.

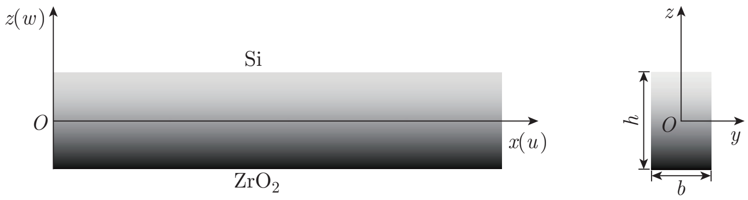

Fig. 1 Coordinates and dimensions of the FGM microbeam

3.2 Material properties of the FGM microbeam

FGM microbeams are usually made of metal-like materials and ceramic. Assume that the volume fractions of FGM beams vary continuously in the thickness direction by power functions. The volume V in which the volume fraction of metal-like materials V_{m} and ceramic V_{c} can be written as

$$V_{\mathrm{m}}(z) = \Big(\frac{h-2z}{2h}\Big)^n, \quad V_{\mathrm{c}}(z) = 1 - V_{\mathrm{m}}(z), \tag{11}$$

where n is the power-law index ($0 \leqslant n < \infty$), which can measure the gradient characteristics by controlling the distributions of constituents in FGM microbeams. When $n = 0$, FGM microbeams degenerate into pure metal-like microbeams, and when $n \to \infty$, they become homogenous ceramic material microbeams.

The power-law index dependence of the metal-like material component V_{m} in the FGM microbeam on various in-planes is shown in Fig. 2, such as the geometric midplane $z = 0$, the plane $z = h/4$, and the plane $z = -h/4$. The larger index n leads to a decrease in the component of the metal-like material. As a consequence, the material properties of metal-like material can be continuously changed in the thickness direction. Therefore, the elastic-plastic, thermo-mechanical property of the FGM microbeam changes continuously from one surface to another.

In the linear rule of mixture, the mechanical property $P(z)$ of FGM microbeams can be written as

$$P(z) = (P_{\mathrm{m}} - P_{\mathrm{c}})V_{\mathrm{m}}(z) + P_{\mathrm{c}}, \tag{12}$$

where P_{m} and P_{c} denote the mechanical properties of metal-like materials and ceramic, respectively. The ceramic material considered is ZrO_2, and the metal-like material is Si. On one

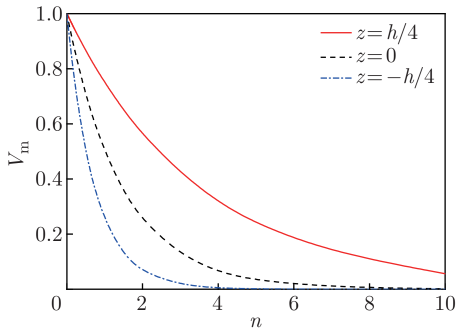

Fig. 2 Power-law index dependence of metal-like component V_m in FGM microbeams (color online)

hand, the metal-like material can increase the electrical and thermal conductivities. On the other hand, the addition of ceramic can improve the corrosion resistance and thermal shock resistance of FGM microbeams.

3.3 Fundamental equations

In the Euler-Bernoulli beam theory, the cross sections remain plane and normal to the longitudinal axis. The displacements can be given by[54–56]

$$u_x = -z\frac{\partial w}{\partial x}, \quad u_y = 0, \quad u_z = w(x,t). \tag{13}$$

Referring to Eq. (7), the strains are

$$\varepsilon_x = -z\frac{\partial^2 w}{\partial x^2}, \quad \varepsilon_y = 0, \quad \varepsilon_z = 0. \tag{14}$$

Combining Eqs. (9) and (14) and neglecting Poisson's effect, we can obtain

$$\Big(1-(e_0a)^2\frac{\partial^2}{\partial x^2}\Big)\sigma_x = E\varepsilon_x - E\alpha_\mathrm{T}\theta = -Ez\frac{\partial^2 w}{\partial x^2} - E\alpha_\mathrm{T}\theta. \tag{15}$$

Similar to the classical beam theory that $M=\int_{-h/2}^{h/2}\sigma_x bz\mathrm{d}z$, multiplying Eq. (15) by $12bz/h^3$ and integrating it with respect to z from $-h/2$ to $h/2$, we can obtain the bending moment

$$M(x,t) = (e_0a)^2\frac{\partial^2 M}{\partial x^2} - EI\Big(\frac{\partial^2 w}{\partial x^2} + \alpha_\mathrm{T}M_\mathrm{T}\Big), \tag{16}$$

where $I = bh^3/12$ is the inertial moment of the cross-section, and M_T is the thermal moment defined by

$$M_\mathrm{T} = \frac{12}{h^3}\int_{-h/2}^{h/2}\theta(x,z,t)z\mathrm{d}z. \tag{17}$$

The motion equation takes the expression as[56]

$$\frac{\partial^2 M}{\partial x^2} = \rho A\frac{\partial^2 w}{\partial t^2}. \tag{18}$$

Substituting Eq. (18) into Eq. (16) yields

$$M(x,t) = (e_0a)^2\rho A\frac{\partial^2 w}{\partial t^2} - EI\Big(\frac{\partial^2 w}{\partial x^2} + \alpha_\mathrm{T}M_\mathrm{T}\Big). \tag{19}$$

Combining Eqs. (18) and (19), the motion equation is obtained as

$$\Big(\frac{\partial^4}{\partial x^4}+\frac{\rho A}{EI}\frac{\partial^2}{\partial t^2}\Big(1-(e_0a)^2\frac{\partial^2}{\partial x^2}\Big)\Big)w+\alpha_{\mathrm{T}}\frac{\partial^2 M_{\mathrm{T}}}{\partial x^2}=0. \tag{20}$$

Combining Eqs. (10) and (14), the energy equation is written as

$$\kappa\Big(\frac{\partial^2\theta}{\partial x^2}+\frac{\partial^2\theta}{\partial z^2}\Big)=\Big(1+\tau_0\frac{\partial}{\partial t}\Big)\Big(\rho c_{\mathrm{E}}\frac{\partial\theta}{\partial t}-\beta T_0 z\frac{\partial}{\partial t}\Big(\frac{\partial^2 w}{\partial x^2}\Big)\Big). \tag{21}$$

For a microbeam, assume that the temperature varies in terms of $\sin(pz)$ along the thickness direction ($p=\pi/h$), that is,

$$\theta(x,z,t)=\Theta(x,t)\sin(pz). \tag{22}$$

Substituting Eq. (22) into Eqs. (19) and (20) yields

$$M(x,t)=(e_0a)^2\rho A\frac{\partial^2 w}{\partial t^2}-EI\Big(\frac{\partial^2 w}{\partial x^2}+\frac{24\alpha_{\mathrm{T}}}{\pi^2 h}\Theta(x,t)\Big), \tag{23}$$

$$\Big(\frac{\partial^4}{\partial x^4}+\frac{\rho A}{EI}\frac{\partial^2}{\partial t^2}\Big(1-(e_0a)^2\frac{\partial^2}{\partial x^2}\Big)\Big)w+\frac{24\alpha_{\mathrm{T}}}{\pi^2 h}\frac{\partial^2\Theta}{\partial x^2}=0. \tag{24}$$

Combining Eqs. (21) and (22), multiplying Eq. (21) by means of $12z/h^3$, and integrating it with respect to z through the microbeam thickness from $-h/2$ to $h/2$, we can obtain

$$\kappa\Big(\frac{\partial^2}{\partial x^2}-p^2\Big)\Theta=\Big(1+\tau_0\frac{\partial}{\partial t}\Big)\Big(\rho c_{\mathrm{E}}\frac{\partial\Theta}{\partial t}-\frac{\beta T_0\pi^2 h}{24}\frac{\partial}{\partial t}\Big(\frac{\partial^2 w}{\partial x^2}\Big)\Big). \tag{25}$$

The following dimensionless variables are introduced for normalization:

$$\begin{cases}(x^*,u^*,w^*,z^*,L^*,h^*,b^*)=c\eta(x,u,w,z,L,h,b), \quad (t^*,t_0^*,\tau_0^*)=c^2\eta(t,t_0,\tau_0),\\ (e_0a)^*=c^2\eta^2(e_0a), \quad \Theta^*=\dfrac{\Theta}{T_0}, \quad \sigma_x^*=\dfrac{\sigma_x}{E}, \quad M^*=\dfrac{M}{c\eta EI}, \quad c=\sqrt{\dfrac{E}{\rho}}, \quad \eta=\dfrac{\rho c_{\mathrm{E}}}{\kappa}.\end{cases} \tag{26}$$

Using the above dimensionless variables, Eqs. (15) and (23)–(25) can be expressed as (dropping the superscript '$*$' for convenience)

$$\Big(1-(e_0a)^2\frac{\partial^2}{\partial x^2}\Big)\sigma_x=-z\frac{\partial^2 w}{\partial x^2}-A_6\Theta\sin(pz), \tag{27}$$

$$M=A_3\frac{\partial^2 w}{\partial t^2}-\frac{\partial^2 w}{\partial x^2}-A_2\Theta, \tag{28}$$

$$\frac{\partial^4 w}{\partial x^4}+A_1\frac{\partial^2 w}{\partial t^2}-A_3\frac{\partial^4 w}{\partial x^2\partial t^2}+A_2\frac{\partial^2\Theta}{\partial x^2}=0, \tag{29}$$

$$\Big(\frac{\partial^2}{\partial x^2}-A_4p^2\Big)\Theta=\Big(1+\tau_0\frac{\partial}{\partial t}\Big)\Big(\frac{\partial\Theta}{\partial t}-A_5\frac{\partial}{\partial t}\Big(\frac{\partial^2 w}{\partial x^2}\Big)\Big), \tag{30}$$

where

$$A_1=\frac{12}{h^2}, \quad A_2=\frac{24T_0\alpha_{\mathrm{T}}}{\pi^2 h}, \quad A_3=\frac{12(e_0a)^2}{h}, \quad A_4=\frac{\pi^2}{h^2}, \quad A_5=\frac{\beta\pi^2 h}{24\kappa\eta}, \quad A_6=\alpha_{\mathrm{T}}T_0.$$

4 Initial and boundary conditions

The initial conditions have the following forms:

$$\begin{cases} w(x,t)|_{t=0} = 0, & \left.\dfrac{\partial w(x,t)}{\partial t}\right|_{t=0} = 0, \\ \Theta(x,t)|_{t=0} = 0, & \left.\dfrac{\partial \Theta(x,t)}{\partial t}\right|_{t=0} = 0. \end{cases} \tag{31}$$

The microbeam is assumed to be simply supported at both ends. Thus, the boundary conditions are

$$w(x,t)|_{x=0,L} = 0, \quad \left.\frac{\partial^2 w(x,t)}{\partial x^2}\right|_{x=0,L} = 0. \tag{32}$$

The microbeam is assumed to be heated by the ramp-type heating at $x = 0$ and heat-insulated at $x = L$,

$$\Theta(x,t)|_{x=0} = \theta_0 \begin{cases} 0, & t \leqslant 0, \\ \dfrac{t}{t_0}, & 0 < t < t_0, \\ 1, & t \geqslant t_0, \end{cases} \quad \left.\frac{\partial \Theta}{\partial x}\right|_{x=L} = 0, \tag{33}$$

where θ_0 is a constant representing the magnitude of the ramp heating, and t_0 is the ramp-heating time parameter.

5 Solutions in the Laplace domain

Applying the Laplace transformation

$$\overline{F}(s) = L(f(t)) = \int_0^\infty \mathrm{e}^{-st} f(t)\mathrm{d}t, \quad \mathrm{Re}(s) > 0 \tag{34}$$

to Eqs. (27)–(30), the following equations are obtained:

$$\Big(1 - (e_0 a)^2 \frac{\mathrm{d}^2}{\mathrm{d}x^2}\Big)\overline{\sigma}_x = \Big(-z\frac{\mathrm{d}^2 w}{\mathrm{d}x^2} - A_6 \overline{\Theta}\sin(pz)\Big), \tag{35}$$

$$\overline{M} = -\Big(\frac{\mathrm{d}^2}{\mathrm{d}x^2} - A_3 s^2\Big)\overline{w} - A_2\overline{\Theta}, \tag{36}$$

$$\Big(\frac{\mathrm{d}^4}{\mathrm{d}x^4} - A_3 s^2 \frac{\mathrm{d}^2}{\mathrm{d}x^2} + A_1 s^2\Big)\overline{w} = -A_2 \frac{\mathrm{d}^2 \Theta}{\mathrm{d}x^2}, \tag{37}$$

$$\Big(\frac{\mathrm{d}^2}{\mathrm{d}x^2} - B_1\Big)\Theta = -B_2 \frac{\mathrm{d}^2 \overline{w}}{\mathrm{d}x^2}, \tag{38}$$

where s is the Laplace transform factor, and

$$B_1 = A_4 + s(1 + \tau_0 s), \quad B_2 = A_5 s(1 + \tau_0 s). \tag{39}$$

In the Laplace domain, the boundary conditions can be obtained as

$$\begin{cases} \overline{w}(x,s)|_{x=0,L} = 0, \quad \left.\dfrac{\mathrm{d}^2 \overline{w}(x,s)}{\mathrm{d}x^2}\right|_{x=0,L} = 0, \\ \overline{\Theta}(x,s)_{x=0} = \theta_0 \Big(\dfrac{1 - \mathrm{e}^{-t_0 s}}{t_0 s^2}\Big) = \overline{g}(s), \\ \left.\dfrac{\partial \overline{\Theta}}{\partial x}\right|_{x=L} = 0. \end{cases} \tag{40}$$

Combining Eqs. (37) and (38), we can obtain

$$\overline{\Theta} = -\frac{1}{A_2 B_1}\Big(\frac{\mathrm{d}^4}{\mathrm{d}x^4} - A_3 s^2 \frac{\mathrm{d}^2}{\mathrm{d}x^2} + A_1 s^2 - A_2 B_2 \frac{\mathrm{d}^2}{\mathrm{d}x^2}\Big)\overline{w}. \tag{41}$$

Substituting Eq. (41) into Eq. (37) and eliminating $\overline{\Theta}$, one can obtain

$$\Big(\frac{\mathrm{d}^6}{\mathrm{d}x^6} - a^* \frac{\mathrm{d}^4}{\mathrm{d}x^4} + b^* \frac{\mathrm{d}^2}{\mathrm{d}x^2} - c^*\Big)\overline{w} = 0, \tag{42}$$

where

$$a^* = A_3 s^2 + A_2 B_2 + B_1, \quad b^* = A_1 s^2 + B_1 A_3 s^2, \quad c^* = A_1 B_1 s^2. \tag{43}$$

Similarly, $\overline{\Theta}$ satisfies

$$\Big(\frac{\mathrm{d}^6}{\mathrm{d}x^6} - a^* \frac{\mathrm{d}^4}{\mathrm{d}x^4} + b^* \frac{\mathrm{d}^2}{\mathrm{d}x^2} - c^*\Big)\overline{\Theta} = 0. \tag{44}$$

Then, Eqs. (42) and (44) can be factorized as

$$((\mathrm{D}^2 - k_1^2)(\mathrm{D}^2 - k_2^2)(\mathrm{D}^2 - k_3^2))(\overline{w}, \overline{\Theta}) = 0, \tag{45}$$

where $\mathrm{D}^2 = \mathrm{d}^2/\mathrm{d}x^2$, and k_1, k_2, and k_3 are the roots with positive real parts of the characteristic equation

$$k^6 - a^* k^4 + b^* k^2 + c^* = 0, \tag{46}$$

where

$$k_1 = \sqrt{\frac{1}{3}(2p^* \sin q^* + a^*)}, \tag{47}$$

$$k_2 = \sqrt{\frac{1}{3}p^*(-(\sqrt{3}\cos q^* - \sin q^*) + a^*)}, \tag{48}$$

$$k_3 = \sqrt{\frac{1}{3}p^*(\sqrt{3}\cos q^* - \sin q^*) + \frac{1}{3}a^*}, \tag{49}$$

$$p^* = \sqrt{a^{*2} - 3b^*}, \quad q^* = \frac{1}{3}\arcsin\Big(\frac{-2a^{*3} + 9a^* b^* - 27c^*}{2p^{*3}}\Big). \tag{50}$$

The solutions to Eqs. (42) and (44) take the forms of

$$\overline{w}(x,s) = \sum_{j=1}^{3}(C_j \mathrm{e}^{-k_j x} + C_{j+3}\mathrm{e}^{k_j x}), \tag{51}$$

$$\overline{\Theta}(x,s) = -\sum_{j=1}^{3} m_j (C_j \mathrm{e}^{-k_j x} + C_{j+3}\mathrm{e}^{k_j x}), \tag{52}$$

where

$$m_j = \frac{B_2 k_j^2}{B_1 - k_j^2}. \tag{53}$$

With the aids of Eqs. (51) and (52), from Eqs. (35) and (36), we can obtain

$$\overline{\sigma}_x(x,s) = \sum_{j=1}^{3}\Big(-zk_j^2 + A_6\sum_{j=1}^{3} m_j \sin(pz)\Big)(C_j \mathrm{e}^{-k_j x} + C_{j+3}\mathrm{e}^{k_j x})/(1-(e_0 a)^2 k_j^2), \tag{54}$$

$$\overline{M}(x,s) = -\sum_{j=1}^{3}(k_j^2 - A_3 s^2 + A_2 m_j)(C_j \mathrm{e}^{-k_j x} + C_{j+3}\mathrm{e}^{k_j x}). \tag{55}$$

With the help of Eq. (51), from Eq. (13), one can obtain

$$\overline{u}(x,s)=-z\frac{\mathrm{d}\overline{w}}{\mathrm{d}x}=z\sum_{j=1}^{3}k_j(C_j\mathrm{e}^{-k_jx}-C_{j+3}\mathrm{e}^{k_jx}). \tag{56}$$

Substituting Eqs. (51) and (52) into Eq. (40) yields

$$\begin{cases} C_1+C_2+C_3+C_4+C_5+C_6=0,\\ C_1\mathrm{e}^{-k_1L}+C_2\mathrm{e}^{-k_2L}+C_3\mathrm{e}^{-k_3L}+C_4\mathrm{e}^{k_1L}+C_5\mathrm{e}^{k_2L}+C_6\mathrm{e}^{k_3L}=0,\\ k_1^2(C_1+C_4)+k_2^2(C_2+C_5)+k_3^2(C_3+C_6)=0,\\ k_1^2(C_1\mathrm{e}^{-k_1L}+C_4\mathrm{e}^{k_1L})+k_2^2(C_2\mathrm{e}^{-k_2L}+C_5\mathrm{e}^{k_2L})+k_3^2(C_3\mathrm{e}^{-k_3L}+C_6\mathrm{e}^{k_3L})=0,\\ m_1(C_1+C_4)+m_2(C_2+C_5)+m_3(C_3+C_6)=\overline{g}(s),\\ m_1(-k_1C_1\mathrm{e}^{-k_1L}+k_1C_4\mathrm{e}^{k_1L})+m_2(-k_2C_2\mathrm{e}^{-k_2L}+k_2C_5\mathrm{e}^{k_2L})\\ \ +m_3(-k_3C_3\mathrm{e}^{-k_3L}+k_3C_6\mathrm{e}^{k_3L})=0. \end{cases} \tag{57}$$

Then, Eq. (57) can be solved to get the coefficients C_j and C_{j+3} $(j=1,2,3)$. Due to the lengthy expressions, they are not presented here.

6 Solutions in the time domain

Because the obtained solutions have lengthy and complex expressions in the Laplace domain, it is difficult to invert them analytically. Alternatively, the numerical inversion can be realized by the algorithm of numerical inversion of the Laplace transform proposed by Brancik[57].

7 Results and discussion

The necessary material properties are specified in Table 1.

Table 1 Material constants of ZrO_2 and Si[58–59]

Material	$\rho/(\mathrm{kg\cdot m^{-3}})$	E/GPa	$\kappa/(\mathrm{W\cdot m^{-1}\cdot K^{-1}})$	$C_{\mathrm{E}}/(\mathrm{J\cdot kg^{-1}\cdot K^{-1}})$	$\alpha_{\mathrm{T}}/\mathrm{K^{-1}}$	ν
ZrO_2	3 657	244.27	1.71	2.74	12.77×10^{-6}	0.29
Si	2 330	169	156	713	2.59×10^{-6}	0.22

The dimensionless geometric variables[60] are $L=1, L/h=10$, and $b/h=0.5$.

In calculation, the effects of the ramp-heating time parameter, the nonlocal parameter, and the power-law index on the dimensionless temperature, the stress, the deflection, and the displacement are examined, respectively.

7.1 The effect of ramp-heating time parameter

In this case, the influence of the ramp-heating time parameter t_0 on the considered variables is examined. In calculation, three different values $t_0=0.01$, $t_0=0.05$, and $t_0=0.1$ are specified, while the nonlocal parameter, the power-law index, and the thermal relaxation time are set as $e_0a=0$, $n=0$, and $\tau_0=0.02$, respectively. The obtained results at $t=0.05$ are illustrated in Figs. 3–6.

Figure 3 shows that the non-zero region of the dimensionless temperature is bounded. Along the x-axis, the dimensionless temperature gradually decreases and approaches zero. Since the time is specified as $t=0.05$, this means that it takes at most the ramp-heating time parameter $t_0=0.05$ for the ramp heating to approach its maximum value $\theta_0=1$. For a larger ramp-heating time parameter $(t_0>t>0)$, i.e., $t_0=0.1$, the maximum value of the dimensionless

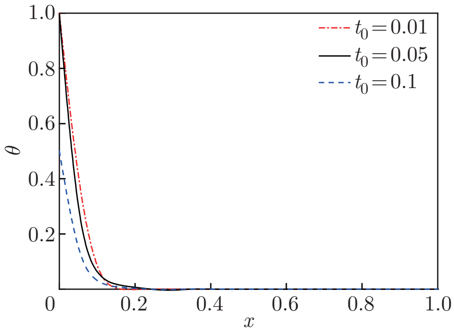

Fig. 3 Distribution of the dimensionless temperature under different values of the ramp-heating time parameter (color online)

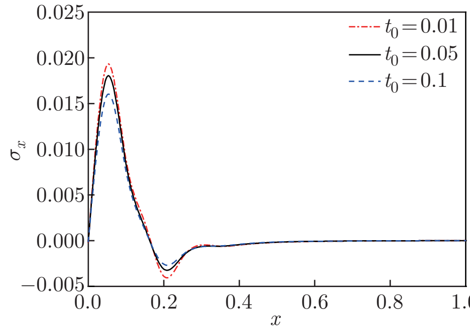

Fig. 4 Distribution of the dimensionless stress under different values of the ramp-heating time parameter (color online)

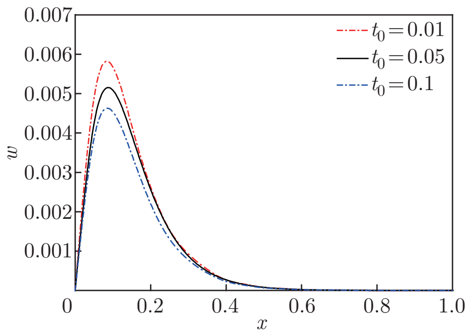

Fig. 5 Distribution of the dimensionless deflection under different values of the ramp-heating time parameter (color online)

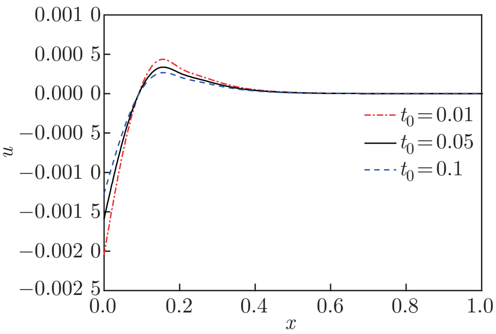

Fig. 6 Distribution of the dimensionless displacement under different values of the ramp-heating time parameter (color online)

temperature is 0.5 which coincides with the thermal boundary condition, while for smaller ramp-heating time parameters ($t \geqslant t_0$), i.e., $t_0 = 0.01$ and $t_0 = 0.05$, the maximum value of the dimensionless temperature is 1. With the increase in the ramp-heating time parameter t_0, the maximum value of the dimensionless temperature decreases.

Figure 4 demonstrates that the dimensionless stress goes up from zero, reaches a positive peak value around $x = 0.05$, afterwards, goes down to the negative peak value around $x = 0.2$, and goes up till zero. A larger t_0 increases the value of the dimensionless stress, which is obvious at the peaks of the curves.

Figure 5 displays that the dimensionless deflection keeps zero at $x = 0$ and $x = 1$, which is consistent with the simply supported boundary condition. The deflection goes up from zero, then reaches a peak value around $x = 0.1$, and afterwards, goes down till zero. With the increase in the ramp-heating time parameter t_0, the value of the dimensionless deflection decreases.

Figure 6 illustrates that the dimensionless displacement goes up from a negative value to a positive value, reaches the peak value, and then goes down till zero. The value of the dimensionless displacement decreases with the increase in the ramp-heating time parameter t_0.

The present work can be reduced to Ref. [61] when $e_0a = 0$ and $n = 0$. In Ref. [61], the thermoelastic response of the nanobeam subject to a ramp-type heating based on the generalized thermoelasticity was solved by the Laplace transform and eigenvalue approach. Although the solving method in the present work is different from that in Ref. [61], the distributions in Figs. 3–6 are basically consistent with those in Ref. [61].

7.2 The effect of the nonlocal parameter

In this case, the influence of the nonlocal parameter e_0a on the considered variables is concerned. We refer to the selection of nonlocal parameters in Refs. [62]–[64], in which the reasonable selection range of the nonlocal parameter is $0 \leqslant e_0a \leqslant 0.1$. In calculation, three different values $e_0a = 0$ (without the nonlocal effect), $e_0a = 0.05$, and $e_0a = 0.1$ are specified while the ramp-heating time parameter, the power-law index, and the thermal relaxation time are set as $t_0 = 0.05$, $n = 0$, and $\tau_0 = 0.02$, respectively. The obtained results at $t = 0.1$ are illustrated in Figs. 7–10.

Figure 7 shows that the nonlocal parameter has no effect on the variation of the dimensionless temperature. In Fig. 8, the peak value of the dimensionless stress decreases with the increase in the nonlocal parameter. Meanwhile, it can be concluded that the nonlocal parameter has a significant effect on the peak value of the dimensionless stress, that is, weakening the stress. This is because the larger lattice constant of a acts to increase the nonlocal effect parameter e_0a, which indicates that the influence of the nonlocal effect on the safety design in micro-scale cannot be ignored.

In Figs. 9 and 10, the peak values of the dimensionless deflection and displacement decrease with the increase in the nonlocal parameter. That is, the nonlocal effect decreases the deforma-

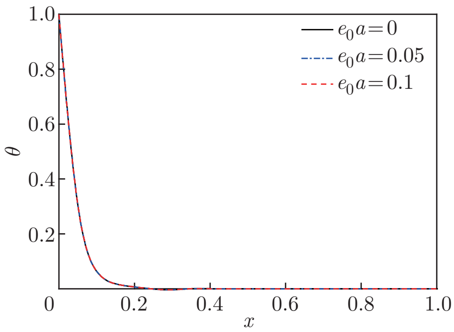

Fig. 7 Distribution of the dimensionless temperature under different values of the nonlocal parameter (color online)

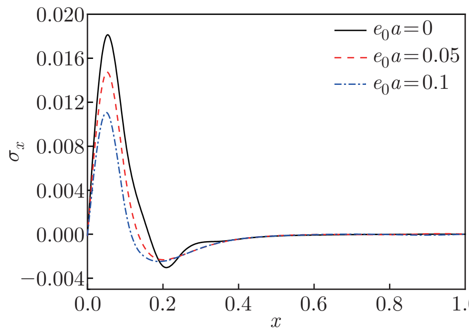

Fig. 8 Distribution of the dimensionless stress under different values of the nonlocal parameter (color online)

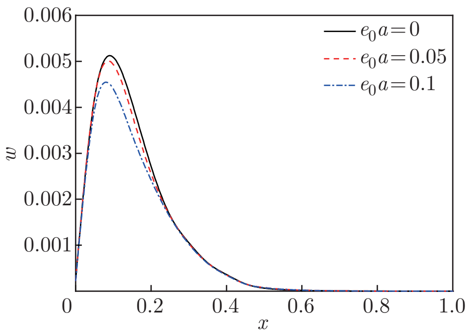

Fig. 9 Distribution of the dimensionless deflection under different values of the nonlocal parameter (color online)

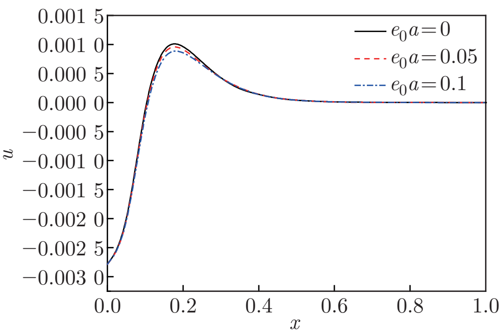

Fig. 10 Distribution of the dimensionless displacement under different values of the nonlocal parameter (color online)

tion of the microbeams. Similar viewpoint can be found in the nonlocal hardening model[65–68].

7.3 The composition effect of FGM

7.3.1 The effect of the power-law index n

In this case, the effect of n on the considered variables is considered. In calculation, seven different values $n = 0$, $n = 0.1$, $n = 0.2$, $n = 0.5$, $n = 1$, $n = 2$, and $n = 5$ are specified while the ramp-heating time parameter, the thermal relaxation time, and the nonlocal parameter are set as $t_0 = 0.05$, $\tau_0 = 0.02$, and $e_0a = 0.05$, respectively. The obtained results at $t = 0.1$ are illustrated in Figs. 11–13.

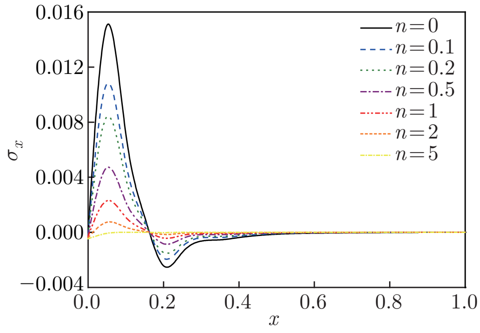

Fig. 11 Distribution of the dimensionless stress under different values of the power-law index (color online)

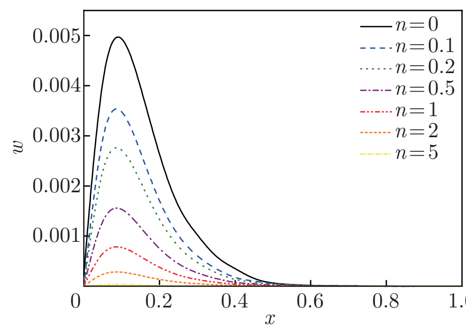

Fig. 12 Distribution of the dimensionless deflection under different values of the power-law index (color online)

Figures 11–13 show that with the increase in the power-law index n, the displacement u, the deflection w, and the stress σ_x decrease. This is because as the index n increases, the composition of Si decreases and the composition of ZrO_2 increases. Due to the increase in the bending stiffness in the FGM microbeam, the load-bearing capacity of the FGM microbeam is greater. Therefore, the ability to resist the thermal-induced stress and deformation is enhanced.

7.3.2 The effect of the power-law index n on the peak values of considered variables

In this case, the effects of the index n on the peak values of considered variables are examined. In calculation, the stress peak position $x = 0.05$, the deflection peak position $x = 0.1$, and the displacement peak position $x = 0$ are specified, while the ramp-heating time parameter, the thermal relaxation time, and the nonlocal parameter are set as $t_0 = 0.05$, $\tau_0 = 0.02$, and $e_0a = 0.05$, respectively. The obtained results at $t = 0.1$ are illustrated in Figs. 14–16.

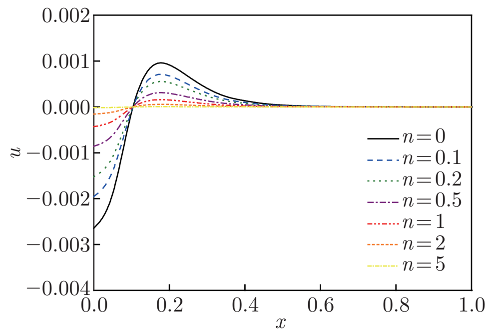

Fig. 13 Distribution of the dimensionless displacement under different values of the power-law index (color online)

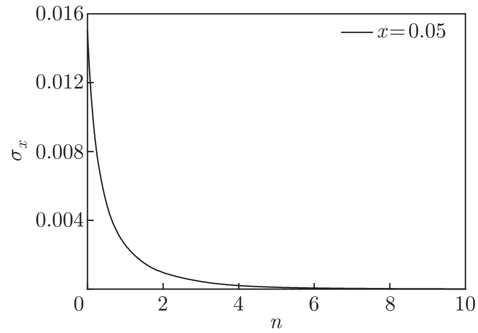

Fig. 14 Stress peak of the FGM microbeam versus the index n

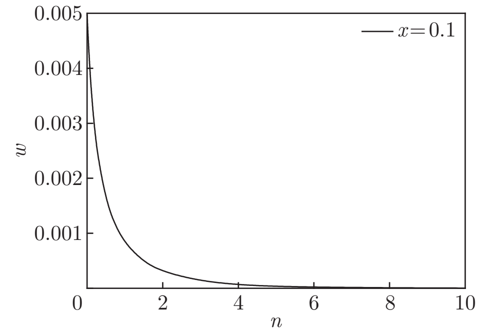

Fig. 15 Deflection peak of the FGM microbeam versus n

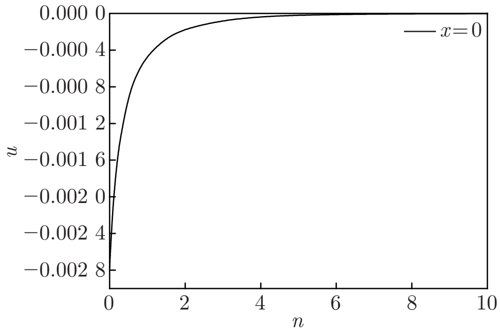

Fig. 16 Displacement peak of the FGM microbeam versus n

Figures 14–16 show that when $n < 1$, the dimensionless stress, the deflection, and the displacement sharply decrease. As n gradually increases, the curves tend to be smooth. Because the addition of ceramic component suddenly increases, the bending stiffness of the homogeneous Si material microbeam increases. Meanwhile, with the gradual increase in n, the bending stiffness gradually approaches a certain value and is close to the elastic deformation of ceramic.

8 Conclusions

The dynamic thermoelastic response of an FGM beam in micro-scale, heated by a ramping type heating at the left end, is investigated in the nonlocal generalized thermoelasticity. From the obtained results, the following conclusions can be drawn.

(i) At a given time, the non-zero regions of the considered variables are bounded, which demonstrates that the thermal wave propagates at a finite speed.

(ii) The nonlocal parameter has no effect on the dimensionless temperature. Meanwhile, it is seen that the stress, deflection, and displacement are reduced due to the existence of the nonlocal parameter. This indicates that the influence of the nonlocal effect on the safety design of microbeam in the thermal environment cannot be ignored.

(iii) As the index n increases, the composition of ceramic increases, and the stiffness and stability of the FGM microbeam increase. Thus, the FGM microbeam with an appropriate amount of ceramic can improve the stiffness and stability of the FGM microbeam.

References

[1] GAYEN, D., TIWARI, R., and CHAKRABORTY, D. Static and dynamic analyses of cracked functionally graded structural components: a review. *Composites Part B*, **173**, 106982 (2019)

[2] GUPTA, A. and TALHA, M. Recent development in modeling and analysis of functionally graded materials and structures. *Progress in Aerospace Sciences*, **79**, 1–14 (2015)

[3] DAI, H. L., RAO, Y. N., and DAI, T. A review of recent researches on FGM cylindrical structures under coupled physical interactions, 2000–2015. *Composite Structure*, **152**, 199–225 (2016)

[4] EOM, K., PARK, H. S., YOON, D. S., and KWON, T. Nanomechanical resonators and their applications in biological/chemical detection: nanomechanics principles. *Physics Reports*, **503**, 115–163 (2011)

[5] LI, Y. L., MEGUID, S. A., FU, Y. M., and XU, D. L. Unified nonlinear quasistatic and dynamic analysis of RF-MEMS switches. *Acta Mechanica*, **224**, 1741–1755 (2013)

[6] CURRANO, L. J., YU, M., and BALACHANDRAN, B. Latching in an MEMS shock sensor: modeling and experiments. *Sensors and Actuators A*, **159**(1), 41–50 (2010)

[7] HUNG, E. S. and SENTURIA, S. D. Extending the travel range of analog-tuned electrostatic actuators. *Journal of Microelectromechanical Systems*, **8**(4), 497–505 (1999)

[8] TORII, A., SASAKI, M., HANE, K., and OKUMA, S. Adhesive force distribution on microstructures investigated by an atomic force microscope. *Sensors and Actuators A*, **44**(2), 153–158 (1994)

[9] YUAN, Y., ZHAO, K., SAHMANI, S., and SAFAEI, B. Size-dependent shear buckling response of FGM skew nanoplates modeled via different homogenization schemes. *Applied Mathematics and Mechanics* (*English Edition*), **41**(4), 587–604 (2020) https://doi.org/10.1007/s10483-020-2600-6

[10] NEJAD, M. Z., HADI, A., and RASTGOO, A. Buckling analysis of arbitrary two-directional functionally graded Euler-Bernoulli nano-beams based on nonlocal elasticity theory. *International Journal of Engineering Science*, **103**, 1–10 (2016)

[11] SAHMANI, S., AGHDAM, M. M., and RABCZUK, T. Nonlinear bending of functionally graded porous micro/nano-beams reinforced with graphene platelets based upon nonlocal strain gradient theory. *Composite Structure*, **186**(11), 68–78 (2018)

[12] ZHANG, P., QING, H., and GAO, C. F. Exact solutions for bending of Timoshenko curved nanobeams made of functionally graded materials based on stress-driven nonlocal integral model. *Composite Structure*, **245**, 112362 (2020)

[13] RAHMANI, O. and PEDRAM, O. Analysis and modeling the size effect on vibration of functionally graded nanobeams based on nonlocal Timoshenko beam theory. *International Journal of Engineering Science*, **77**(7), 55–70 (2014)

[14] NEJAD, M. Z. and HADI, A. Non-local analysis of free vibration of bi-directional functionally graded Euler-Bernoulli nano-beams. *International Journal of Engineering Science*, **105**, 1–11 (2016)

[15] FLECK, N., MULLER, G., ASHBY, M., and HUTCHINSON, J. Strain gradient plasticity: theory and experiment. *Acta Metallurgica et Materialia*, **42**(2), 475–487 (1994)

[16] NIX, W. D. Mechanical properties of thin films. *Metallurgical and Materials Transactions A*, **20**(11), 2217–2245 (1989)

[17] MA, Q. and CLARKE, D. R. Size dependent hardness of silver single crystals. *Journal of Materials Research*, **10**(4), 853–863 (1995)

[18] STÖLKEN, J. and EVANS, A. A microbend test method for measuring the plasticity length-scale. *Acta Materialia*, **46**(14), 5109–5115 (1998)

[19] CHONG, A. C. M. and LAM, D. C. C. Strain gradient plasticity effect in indentation hardness of polymers. *Journal of Material Research*, **14**(10), 4103–4110 (1999)

[20] ZHAO, M. H., SLAUGHTER, W. S., LI, M., and MAO, S. X. Material-length-scale-controlled nanoindentation size effects due to strain-gradient plasticity. *Acta Materialia*, **51**(15), 4461–4469 (2003)

[21] BEEGAN, D., CHOWDHURY, S., and LAUGIER, M. T. Modification of composite hardness models to incorporate indentation size effects in thin films. *Thin Solid Films*, **516**(12), 3813–3817 (2008)

[22] YU, Q., SHAN, Z. W., LI, J., HUANG, X. X., XIAO, L., SUN, J., and MA, E. Strong crystal size effect on deformation twinning. *nature*, **463**(7279), 335–338 (2010)

[23] MARANGANTI, R. and SHARMA, P. Length scales at which classical elasticity breaks down for various materials. *Physical Review Letters*, **98**(19), 195504 (2007)

[24] ERINGEN, A. C. *Nonlocal Continuum Field Theories*, Springer-Verlag, New York (2002)

[25] AIFANTIS, E. C. Gradient deformation models at nano, micro and macro scales. *Journal of Engineering Materials Technology*, **121**(2), 189–202 (1999)

[26] YANG, F., CHONG, A. C. M., LAM, D. C. C., and TONG, P. Couple stress based strain gradient theory for elasticity. *International Journal of Solids Structures*, **39**(10), 2731–2743 (2002)

[27] PEDDIESON, J., BUCHANAN, G. R., and MCNITT, R. P. Application of nonlocal continuum models to nanotechnology. *International Journal of Engineering Science*, **41**, 305–312 (2002)

[28] AREFI, M. and ZENKOUR, A. M. Influence of micro-length-scale parameter and inhomogeneities on the bending, free vibration and wave propagation analyses of an FG Timoshenko's sandwich piezoelectric microbeam. *Journal of Sandwich Structures and Materials*, **21**(4), 1243–1270 (2019)

[29] GHADIRI, M., HOSSEINI, S. H. S., and SHAFIEI, N. A power series for vibration of a rotating nanobeam with considering thermal effect. *Mechanics of Advanced Materials and Structures*, **23**(12), 1414–1420 (2016)

[30] REDDY, J. N. Nonlocal nonlinear formulations for bending of classical and shear deformation theories of beams and plates. *International Journal of Engineering Science*, **48**, 1507–1518 (2010)

[31] LIM, C. W. and YANG, Y. New predictions of size-dependent nanoscale based on nonlocal elasticity for wave propagation in carbon nanotubes. *Journal of Computational and Theoretical Nanoscience*, **7**(6), 988–995 (2010)

[32] WANG, Q. and VARADAN, V. K. Application of nonlocal elastic shell theory in wave propagation analysis of carbon nanotubes. *Smart Material and Structures*, **16**(1), 178–190 (2007)

[33] WANG, Q. Wave propagation in carbon nanotubes via nonlocal continuum mechanics. *Journal of Applied Physics*, **98**(12), 124301 (2005)

[34] BIOT, M. A. Thermoelasticity and irreversible thermodynamics. *Journal of Applied Physics*, **27**(3), 240–253 (1956)

[35] PESHKOV, V. Second sound in helium. *Journal of Physical*, **8**, 381–386 (1944)

[36] CATTANEO, C. A form of heat conduction equation which eliminates the paradox of instantaneous propagation. *Comptes Rendus Physique*, **247**, 431–433 (1958)

[37] LORD, H. W. and SHULMAN, Y. A. A generalized dynamical theory of thermoelasticity. *Journal of the Mechanics and Physics of Solids*, **15**, 299–309 (1967)

[38] GREEN, A. E. and LINDSAY, K. A. Thermoelasticity. *Journal of Elasticity*, **2**, 1–7 (1972)

[39] GREEN, A. E. and NAGHDI, P. M. Thermoelasticity without energy dissipation. *Journal of Elasticity*, **31**, 189–208 (1993)

[40] GREEN, A. E. and NAGHDI, P. M. On undamped heat waves in an elastic solid. *Journal of Thermal Stresses*, **15**(2), 253–264 (1992)

[41] MA, Y. B. and PENG, W. Dynamic response of an infinite medium with a spherical cavity on temperature-dependent properties subjected to a thermal shock under fractional-order theory of thermoelasticity. *Journal of Thermal Stresses*, **41**(3), 302–312 (2018)

[42] HE, S. Q., PENG, W., MA, Y. B., and HE, T. H. Investigation on the transient response of a porous half-space with strain and thermal relaxations. *European Journal of Mechanics A-Solids*, **84**, 104064 (2020)

[43] ABOUELREGAL, A. E. Size-dependent thermoelastic initially stressed micro-beam due to a varying temperature in the light of the modified couple stress theory. *Applied Mathematics and Mechanics* (*English Edition*), **41**(12), 1805–1820 (2020) https://doi.org/10.1007/s10483-020-2676-5

[44] HE, T. H., LI, C. L., and SHI, S. H. A two-dimensional generalized thermoelastic diffusion problem for a half-space. *European Journal of Mechanics A-Solids*, **52**(12), 37–43 (2015)

[45] LI, C. L., GUO, H. L., and TIAN, X. G. Soret effect on the shock responses of generalized diffusion-thermoelasticity. *Journal of Thermal Stresses*, **40**(12), 1563–1574 (2017)

[46] ELHAGARY, M. A. A two-dimensional generalized thermoelastic diffusion problem for a thick plate subjected to thermal loading due to laser pulse. *Journal of Thermal Stresses*, **37**(12), 1416–1432 (2014)

[47] BEREZOVSKI, A., ENGELBRECHT, J., and MAUGIN, G. A. Thermoelastic wave propagation in inhomogeneous media. *Archive of Applied Mechanics*, **70**(10), 694–706 (2000)

[48] KUMAR, R. and DESWAL, S. Surface wave propagation in a micropolar thermoelastic medium without energy dissipation. *Journal of Sound and Vibration*, **256**(1), 173–178 (2002)

[49] HE, T. H., TIAN, X. G., and SHEN, Y. P. A generalized electromagneto-thermoelastic problem for an infinitely long solid cylinder. *European Journal of Mechanics A-Soilds*, **24**(2), 349–359 (2005)

[50] NAYFEH, A. H. and NEMAT-NASSER, S. Electromagneto-thermoelastic plane waves in solids with thermal relaxation. *Journal of Applied Mechanics*, **39**(1), 108–113 (1972)

[51] MA, Y. B. and HE, T. H. The transient response of a functionally graded piezoelectric rod subjected to a moving heat source under fractional order theory of thermoelasticity. *Mechanics of Advanced Materials and Structures*, **24**(9), 789–796 (2017)

[52] LI, Y. and HE, T. H. The transient response of a functionally graded half-space heated by a laser pulse based on the generalized thermoelasticity with memory dependent derivative. *Mechanics of Advanced Materials and Structures* (2020) https://doi.org/10.1080/15376494.2020.1731888

[53] YU, Y. J., TIAN, X. G., and XIONG, Q. L. Nonlocal thermoelasticity based on nonlocal heat conduction and nonlocal elasticity. *European Journal of Mechanics A-Soilds*, **60**, 238–253 (2016)

[54] XI, Y. Y., LYU, Q., ZHANG, N. H., and WU, J. Z. Thermal-induced snap-through buckling of simply-supported functionally graded beams. *Applied Mathematics and Mechanics* (*English Edition*), **41**(12), 1821–1832 (2020) https://doi.org/10.1007/s10483-020-2691-7

[55] NEJAD, M. Z. and HADI, A. Eringen's non-local elasticity theory for bending analysis of bi-directional functionally graded Euler-Bernoulli nano-beams. *International Journal of Engineering Science*, **106**, 1–9 (2016)

[56] LI, S. R., XU, X., and CHEN, S. Analysis of thermoelastic damping of functionally graded material resonators. *Composite Structures*, **182**, 728–736 (2017)

[57] BRANCIK, L. Programs for fast numerical inversion of Laplace transforms in Matlab language environment. *Proceedings of the 7th Conference MATLAB* 99, Czech Republic, Prague, 27–39 (1999)

[58] HUANG, H. W. and HAN, Q. Nonlinear buckling and postbuckling of heated functionally graded cylindrical shells under combined axial compression and radial pressure. *International Journal of Non-Linear Mechanics*, **44**(2), 209–218 (2009)

[59] NEMAT-ALLA, M., AHMED, K. I. E., and HASSAB-ALLAH, I. Elastic-plastic analysis of two-dimensional functionally graded materials under thermal loading. *International Journal of Solids and Structures*, **46**(14), 2774–2786 (2009)

[60] SUN, Y. X., FANG, D. N., SAKA, M., and SOH, A. K. Laser-induced vibrations of micro-beams under different boundary conditions. *International Journal of Solids and Structures*, **45**(7), 1993–2013 (2008)

[61] YOUSSEF, H. M. and ELSIBAL, K. A. State-space approach to vibration of gold nano-beam induced by ramp type heating. *Nano-Micro Letters*, **2**(3), 139–148 (2010)

[62] YU, Y. J., TIAN, X. G., and LIU, X. R. Size-dependent generalized thermoelasticity using Erigen's nonlocal model. *European Journal of Mechanics A/Solids*, **51**, 96–106 (2015)

[63] ZHANG, P. and HE, T. H. A generalized thermoelastic problem with nonlocal effect and memory-dependent derivative when subjected to a moving heat source. *Wave in Random and Complex Media*, **30**(1), 142–156 (2020)

[64] LI, C. L., GUO, H. L., and TIAN, X. G. Shock-induced thermal wave propagation and response analysis of a viscoelastic thin plate under transient heating loads. *Wave in Random and Comples Media*, **28**(2), 270–286 (2018)

[65] LIM, C. W., LI, C., and YU, J. L. Dynamic behaviour of axially moving nanobeams based on nonlocal elasticity approach. *Acta Mechanica Sinica*, **26**(5), 755–765 (2010)

[66] LIM, C. W. On the truth of nanoscale for nanobeams based on nonlocal elastic stress field theory: equilibrium, governing equation and static deflection. *Applied Mathematics and Mechanics* (*English Edition*), **31**(1), 37–54 (2010) https://doi.org/10.1007/s10483-010-0105-7

[67] LI, C., LIM, C. W., and YU, J. L. Twisting statics and dynamics for circular elastic nanosolids by nonlocal elasticity theory. *Acta Mechanica Solida Sinica*, **24**(6), 484–494 (2011)

[68] LI, C., YAO, L. Q., CHEN, W. Q., and LI, S. Comments on nonlocal effects in nano-cantilever beams. *International Journal of Engineering Science*, **87**, 47–57 (2015)